3.2.3. Ground Model

The soil is classified into 4 types, i.e. clayey soil, sandy soil, sand and clay (mixture or alternation), and gravelly soil. Each soil type is divided into 4 groups according to its N values, as shown in Table 3.2.1. Based on the depth of the seismic bedrock and the soil condition above the bedrock, the ground is classified into 41 types as shown in

Figure 3.2.6. The distribution of each soil type is shown in Figure 3.2.7.

The characteristics of the ground condition in the Study Area are as follows:

- Many types of soil such as gravel, sand, silt and clay are distributed in the Study Area. Most of the soil are overconsolidated and cemented. The engineering characters of these soil types are very similar to each other. Geological structure is simple and soil properties are relatively homogeneous.
- Near ground surface (GL-0 to 30m), soft clay, silt and loose sand are distributed in the alluvial plain. This soft deposit is regarded as the youngest deposit, namely $\boldsymbol{D_1}$ formation.
- Below the $\boldsymbol{D_1}$ formation, a very thick clay layer is deposited at the eastern plain of the Study Area. This layer is regarded as the ***Bs*** formation. The bottom of this formation could not be confirmed with 200m-deep boreholes. The strength of the soil increases gradually in its depth direction. Some relatively soft clay and/or sandy clay layers are embedded in the layer. The thickness of these layers is a few meters.
- Basically, the $\boldsymbol{D_1}$ formation is composed of relatively soft silt and clay. The particle size of this formation becomes coarser toward the alluvial plain edge. Alternation and/or mixture of sand and clay are predominant in this area and these are considered as the transition zone between $\boldsymbol{D_1}$ and $\boldsymbol{D_2}$ formations.
- Most parts of the ***C***, $\boldsymbol{B_n}$ and ***A*** formations are composed of dense gravel with sand and clay. Soft to stiff clay or loose sand is distributed in the Darrus and Qolhak areas, both in north central Tehran. This layer is considered as the lacustrine sediment of an old lake in this area.

Table 3.2.1 Soil Condition, Symbols and N Values for the Ground Model

Soil Name	Soft Clay	Firm Clay	Hard Clay	Very Hard Clay
Symbol	C1	C2	C3	C4
Average N Value	15	35	75	100
Soil Name	Soft Clay and Sand	Firm Clay and Sand	Hard Clay and Sand	Very Hard Clay and Sand
Symbol	CS1	CS2	CS3	CS4
Average N Value	15	35	75	100
Soil Name	Loose Sand	Medium Dense Sand	Dense Sand	Very Dense Sand
Symbol	S1	S2	S3	S4
Average N Value	15	35	75	100
Soil Name	Loose Gravel	Medium Dense Gravel	Dense Gravel	Very Dense Gravel
Symbol	G1	G2	G3	G4
Average N Value	15	35	75	100

Model No.	Depth (GL-m)																									
	5	10	15	20	25	30	35	40	45	50	55	60	65	70	75	80	85	90	95	100	110	120	130	140	150	
1	C1	C1	C1	C1	C1	C1	CS3	CS3	CS3	CS3	C3	C3	C3	C3	C3	C3	C3	C3	C3	C3	C3	C3	C3	C3	C3	C4
2	C1	C1	C2	C2	C2	C2	CS3	CS3	CS3	CS3	C3	C3	C3	C3	C3	C3	C3	C3	C3	C3	C3	C3	C3	C3	C3	C4
3	C1	C1	CS1	CS1	CS1	CS1	CS3	CS3	CS3	CS3	C3	C3	C3	C3	C3	C3	C3	C3	C3	C3	C3	C3	C3	C3	C3	C4
4	C1	C1	C2	C2	C2	C2	C2	C2	C2	C2	C3	C3	C3	C3	C3	C3	C3	C3	C3	C3	C3	C3	C3	C3	C3	C4
5	C1	C1	C1	C1	C1	C1	C2	C2	C2	C2	C3	C3	C3	C3	C3	C3	C3	C3	C3	C3	C3	C3	C3	C3	C3	C4
6	C2	C2	C2	C2	C2	C2	CS3	CS3	CS3	CS3	CS3	CS3	CS3	CS3	CS3	CS3	C2	C2	C2	C2	C2	C2	C2	C2	C2	C4
7	C1	C1	C2	C2	C2	C2	C2	C2	C2	C2	C3	C3	C3	C3	C4											
8	C1	C1	C2	C2	C2	C2	CS2	CS2	CS2	CS2	CS3	CS3	CS3	CS3	C4											
9	C2	C2	CS2	CS2	CS2	CS2	C3	C3	C3	C3	C2	C2	C2	C2	C4											
10	C1	C1	CS2	CS2	CS2	CS2	C3	C3	C3	C3	C2	C2	C2	C2	C4											
11	C2	C2	C3	C3	C3	C3	CS3	CS3	CS3	CS3	C2	C2	C2	C2	C4											
12	C2	C2	C2	C2	C2	C2	C2	C2	C2	C2	C4															
13	C2	C2	C2	C2	C2	C2	CS3	CS3	CS3	CS3	CS4															
14	C2	C2	C2	C2	C2	C2	CS2	CS2	CS2	CS2	CS4															
15	CS1	CS1	C2	C2	C2	C2	CS3	CS3	CS3	CS3	CS4															
16	C2	C2	C2	C2	C2	C2	CS3	CS3	CS3	CS3	CS4															
17	C2	C2	CS1	CS1	CS1	CS1	CS3	CS3	CS3	CS3	CS4															
18	G2	G2	CS1	CS1	CS1	CS1	G3	G3	G3	G3	G4															
19	C3	C3	C3	C3	C3	C3	G3	G3	G3	G3	G4															
20	C2	C2	C3	C3	C3	C3	CS3	CS3	CS3	CS3	CS4															
21	CS2	CS2	CS3	CS3	CS3	CS3	CS3	CS3	CS3	CS3	CS4															
22	C1	C1	C1	C1	C1	C1	C4																			
23	C2	C2	C2	C2	C2	C2	C4																			
24	CS2	CS2	CS2	CS2	CS2	CS2	CS4																			
25	C1	C1	CS2	CS2	CS2	CS2	CS4																			
26	CS1	CS1	CS3	CS3	CS3	CS3	CS4																			
27	G2	G2	G4	G4	G3	G3	G4																			
28	C2	C2	G3	G3	G3	G4																				
29	S3	S3	S3	S3	S3	G4																				
30	S3	S3	G3	G3	G3	G4																				
31	G3	G3	G3	G3	G3	G4																				
32	G2	G2	G3	G3	G4																					
33	G3	G3	G3	G3	G4																					
34	G3	G3	G3	G4																						
35	S3	S3	S3	G4																						
36	CS3	CS3	CS3	G4																						
37	C1	C1	C1	G4																						
38	C2	C2	C2	G4																						
39	G3	G3	G4																							
40	Pre-Miocene																									
41	Rock																									

Soil Name, Symbol and N Value

Clay	C1	C2	C3	C4
Average N Value	15	35	75	100
Sand and Clay	**CS1**	**CS2**	**CS3**	**CS4**
Average N Value	15	35	75	100
Sand	**S1**	**S2**	**S3**	**S4**
Average N Value	15	35	75	100
Gravel	**G1**	**G2**	**G3**	**G4**
Average N Value	15	35	75	100

G4 Engineering seismic bedrock and its soil type

Figure 3.2.6 Model Geological Log

Figure 3.2.7

Model Ground for Seismic Analysis

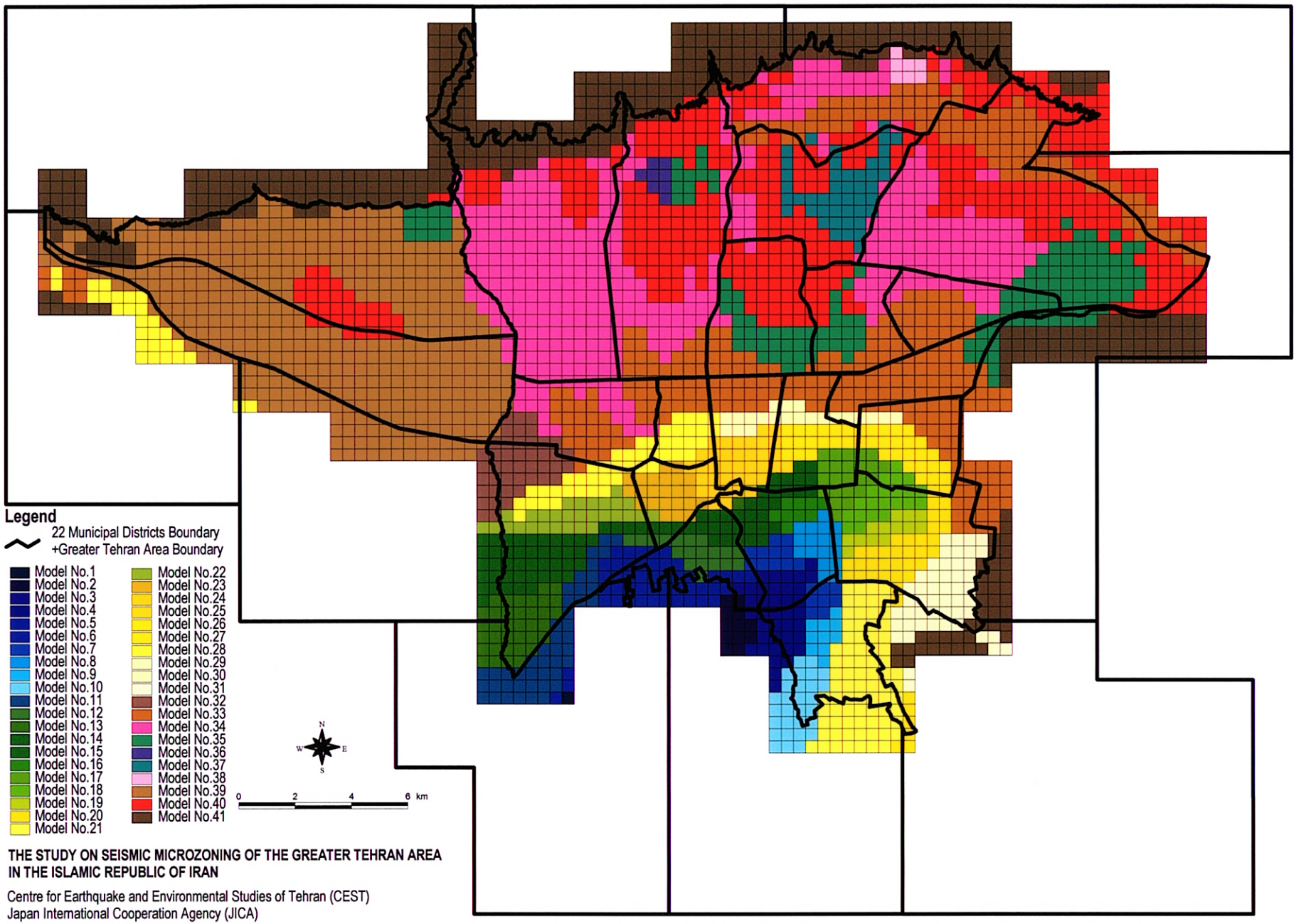

THE STUDY ON SEISMIC MICROZONING OF THE GREATER TEHRAN AREA IN THE ISLAMIC REPUBLIC OF IRAN

Centre for Earthquake and Environmental Studies of Tehran (CEST)
Japan International Cooperation Agency (JICA)

3.2.4. Soil Properties of the Ground Model

(1) Wet Density

Figure 3.2.8 shows the distribution of the wet density by depth. The model property used for the earthquake analysis is defined as shown in Table 3.2.2 for each soil type. The wet density for gravelly soil is estimated from the specific gravity of soil, the moisture content and the density of clayey or sandy soil.

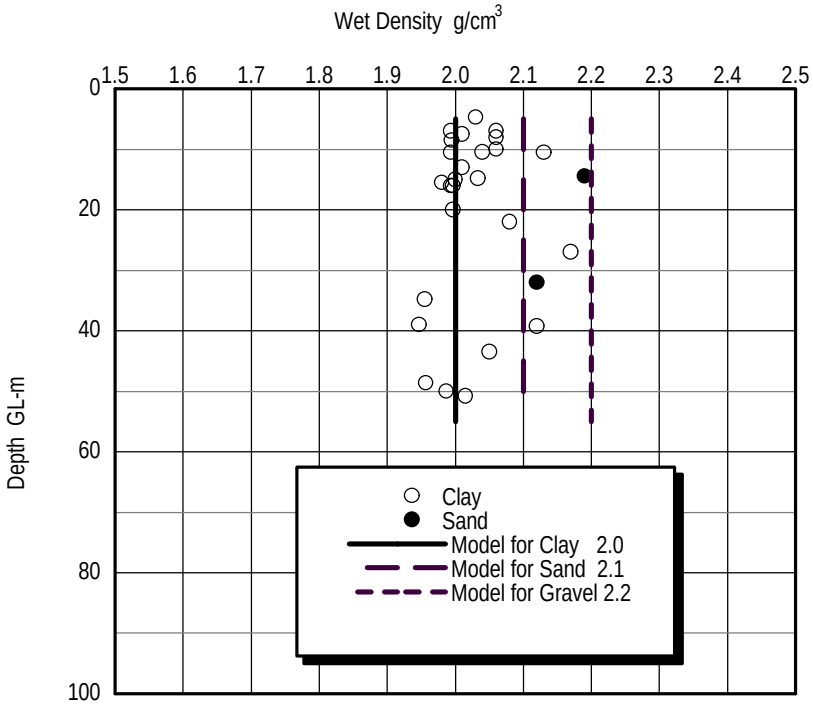

Figure 3.2.8 Relationship between Depth and Wet Density of Soil

(Result of geological site investigation of the Study)

Table 3.2.2 Density of Soil Applied in Earthquake Analysis

Soil Type	Density (g/cm3)
Clayey Soil, Sandy Clayey Soil	2.0
Sandy Soil	2.1
Gravelly Soil	2.2

(2) Shear Wave Velocity

Figure 3.2.9 shows the relation between the N value of the standard penetration test and the shear wave velocity, Vs. The N value is calculated as the equivalent to a 30 cm penetration value Neq. Data for Neq values above 200 are excluded. Some scattered and linear relationship between the Neq and Vs values on a logarithmic scale is observed against the full range of Neq values. This relation is not dependent on soil type. The two parameters are

correlated using the least square method and the following equation is defined as an input parameter for earthquake analysis:

$Vs=161N_{eq}^{0.277}$ (m/sec) ($N_{eq}<200$)

Relational expressions for Vs and the N value used in the Japanese Design Manual for Bridge are also shown in the figure. The equations are as follows:

Clayey Soil $Vs=102N^{0.29}$ ($N<50$)

Sandy Soil $Vs=81N^{0.33}$ ($N<50$)

Compared to the shear wave velocity of Japanese soil, that of the Study Area shows a bigger value. In Japan, the relationships are defined using mainly soft to medium soft soil, of which the N value is less than 50. On the other hand, the soil in Tehran area is much more overconsolidated, N value of which is up to 200.

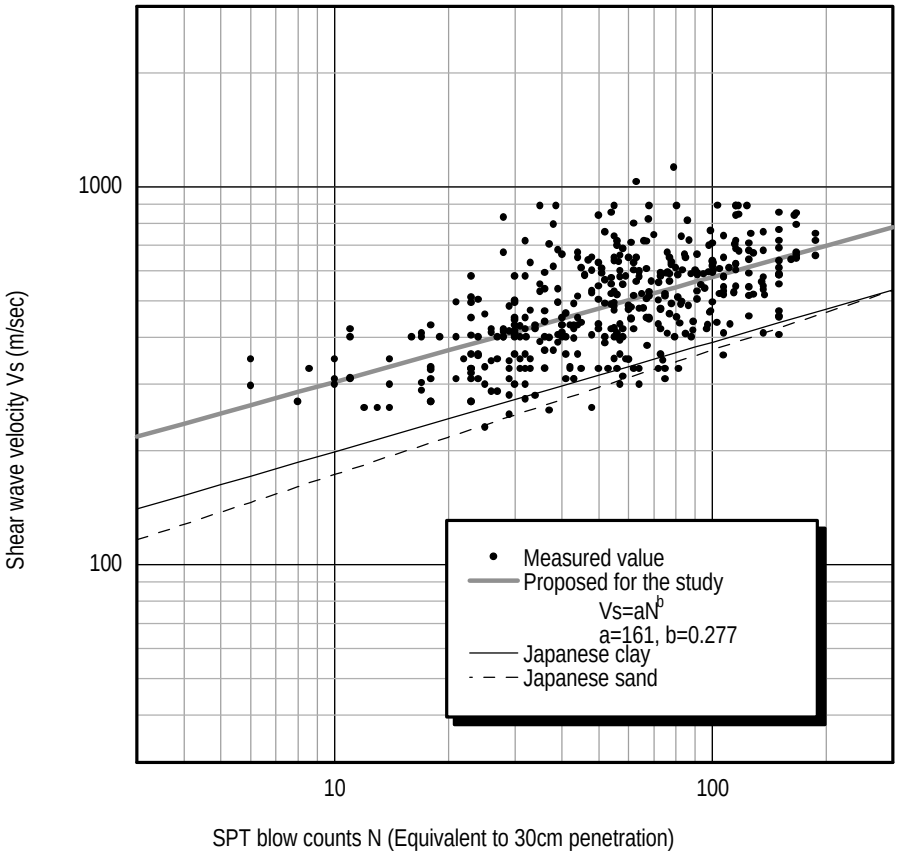

Figure 3.2.9 Relation between SPT Blow Counts and Shear Wave Velocity of Ground

(Result of geological site investigation of the Study)

References for section 3.2

ISSMFE, 1993, Manual for Zonation on Seismic Geotechnical Hazards, Technical Committee for Earthquake Geotechnical Engineering, TC4, International Society of Soil Mechanics and Foundation Engineering.

3.3. Earthquake Scenario

3.3.1. Scenario Earthquake

(1) Concept

Applying a scenario earthquake can be very useful to a city for emergency response and seismic disaster prevention planning. Therefore, the earthquake that would severely damage Tehran should be assumed.

The earthquake that would affect Tehran would occur on an active fault near the city. The severely damaged area would be limited, compared to the case of a huge earthquake of inter-plate subduction type. Tehran is wide enough that it is most probable that one area of the city would suffer from severe damage and other areas would have less damage. It is very important to consider such a situation in the preparation of an emergency response plan. From this point of view, several scenario earthquakes were proposed for use in the Study.

(2) Approach

There are two approaches to estimate strong ground motion: the probabilistic approach and deterministic approach. In the probabilistic approach, peak ground acceleration (PGA) distribution is calculated based on the statistical analysis of available earthquake catalogue entries for a certain return period. An analysis was performed by CEST. PGA at the centre of the city of Tehran was calculated as about 200 gal for a 100-year return period. The meaning of this estimated value is that this location of the city will suffer over 200 gals of strong motion at least once in 100 years. The value itself is useful for each location in the city. However, distribution and amount of damage will not be sufficiently estimated for the earthquake scenario because the distribution of damage will be influenced by many other factors. For this reason, the latter deterministic approach is recommended. There are a number of faults mapped in the Tehran area. Many of them are classified as Quaternary active faults. Recurrence intervals and the latest events have not been investigated in detail, and it is difficult to determine when the scenario earthquake will occur using the deterministic approach. Therefore, a hypothesis based on a worst damage scenario is considered as a basic and indispensable approach to assess the earthquake resistance of the city.

(3) Historical earthquake

Fortunately, Tehran has not suffered any severe damage due to an earthquake in over 150 years. Some earthquakes that might have affected the Tehran area were picked out from the historical earthquake catalogue. These are shown in Table 3.3.1 and Figure 3.3.1. Surface wave magnitudes (Ms) and body wave magnitudes (mb) are converted to the moment magnitude (Mw) according to Utsu (1982). The relation is shown in Figure 3.3.2.

Due to the spatial extent of the Greater Tehran Area, a sample site was selected for peak ground acceleration (PGA) computations. This point was the centre of the city of Tehran. It is near Ferdowsi Square and a highly populated area. Its latitude is 35.70N and its longitude is 51.45E. PGA was calculated according to Campbell et al. (1997) for a dip-slip type earthquake and alluvial ground conditions. Radius or distance was assumed as infinite.

The largest observed PGA was 412 gal due to the earthquake in 855. The second-largest acceleration occurred in 1830, and the third in 958. Berberian et al. (1999) suggested that the events in the years 958, 1830 and 1665 occurred on segments of the Mosha Fault. It has also been suggested that the event in 855 may have occurred at the South/North Ray Fault. Seismic activity on the North Tehran Fault is vague. Berberian et al. (1983) associated the events in 958 and 1177 to the North Tehran Fault.

Table 3.3.1 Historical earthquakes affected to Tehran

year	month	day	Mw	Latitude (degrees)	Longitude (degrees)	Epicentral distance (km)	Assumed PGA (gal)
743			7.1	35.30	52.20	81	49
855			***7.0***	***35.60***	***51.50***	***12***	***412***
856	12	22	7.9	36.20	54.30	263	17
864	1		5.4	35.70	51.00	41	34
958	***2***	***23***	***7.7***	***36.00***	***51.10***	***46***	***161***
1119	12	10	6.4	35.70	49.90	140	13
1177	***5***		***7.1***	***35.70***	***50.70***	***68***	***63***
1301			6.6	36.10	53.20	164	12
1485	8	15	7.1	36.70	50.50	140	23
1608	4	20	7.6	36.40	50.50	116	44
1665			6.4	35.70	52.10	59	44
1687			6.4	36.30	52.60	123	15
1809			6.4	36.30	52.50	116	17
1825			6.6	36.10	52.60	113	21
1830	***3***	***27***	***7.0***	***35.80***	***51.70***	***25***	***208***
1868	8	1	6.3	34.90	52.50	130	13
1930	10	2	5.4	35.78	52.02	52	24
1957	7	2	6.7	36.20	52.60	118	21
1962	9	1	7.1	35.54	49.39	187	15
1983	3	26	5.3	36.12	52.21	83	10
1990	6	20	7.4	36.96	49.39	232	14
1994	11	21	4.5	35.90	51.88	45	14

Source: List from Moinfar et al. (1994)

Note: Location of 1830 earthquake is quoted from Berberian et al.(1999)
Moment Magnitude(Mw), epicentral distance and PGA value were calculated by the Study Team.
Epicentre of italicised earthquake was shown in Figure 3.3.1.

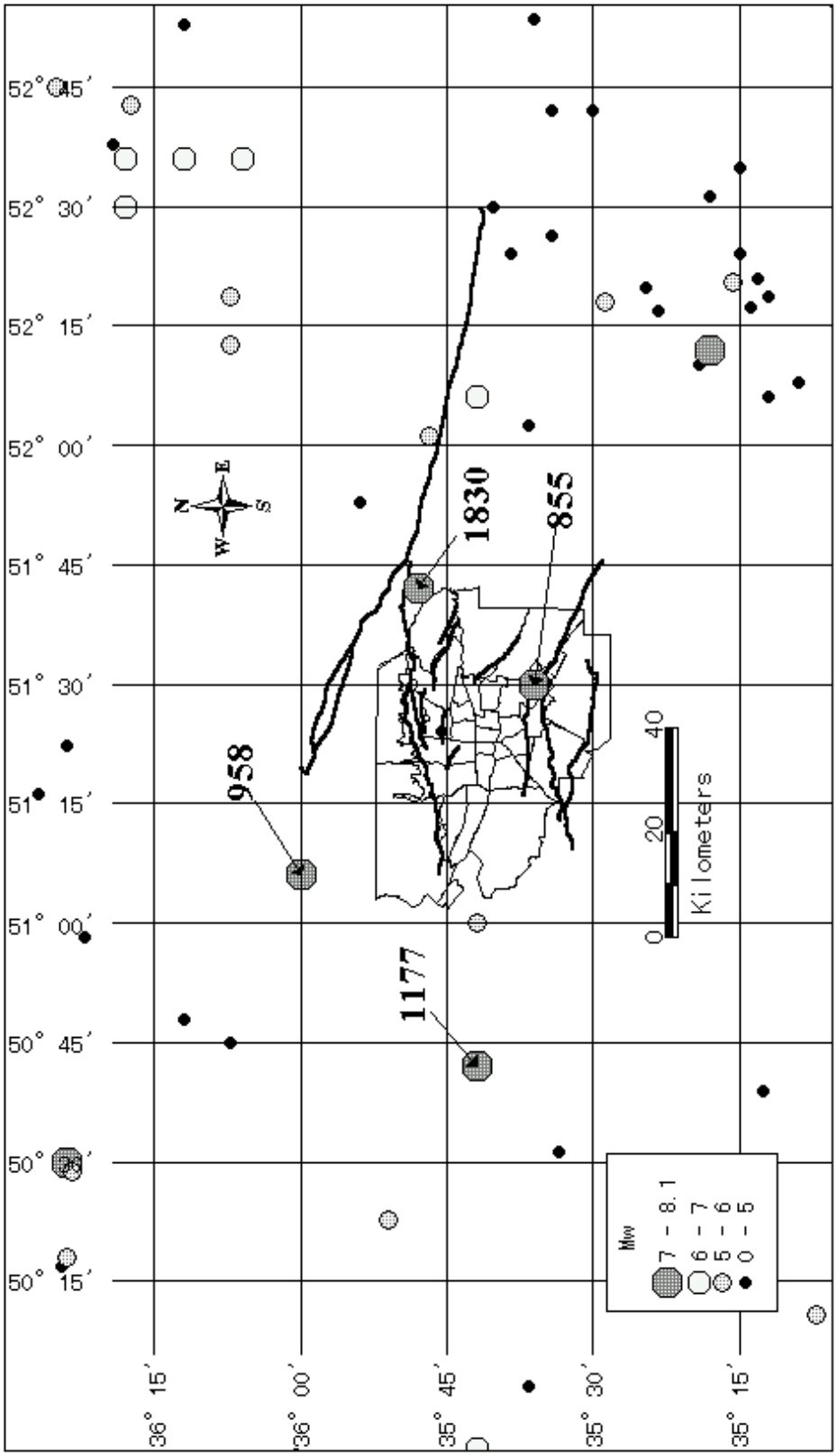

Figure 3.3.1 Historical Earthquake Distribution around Tehran

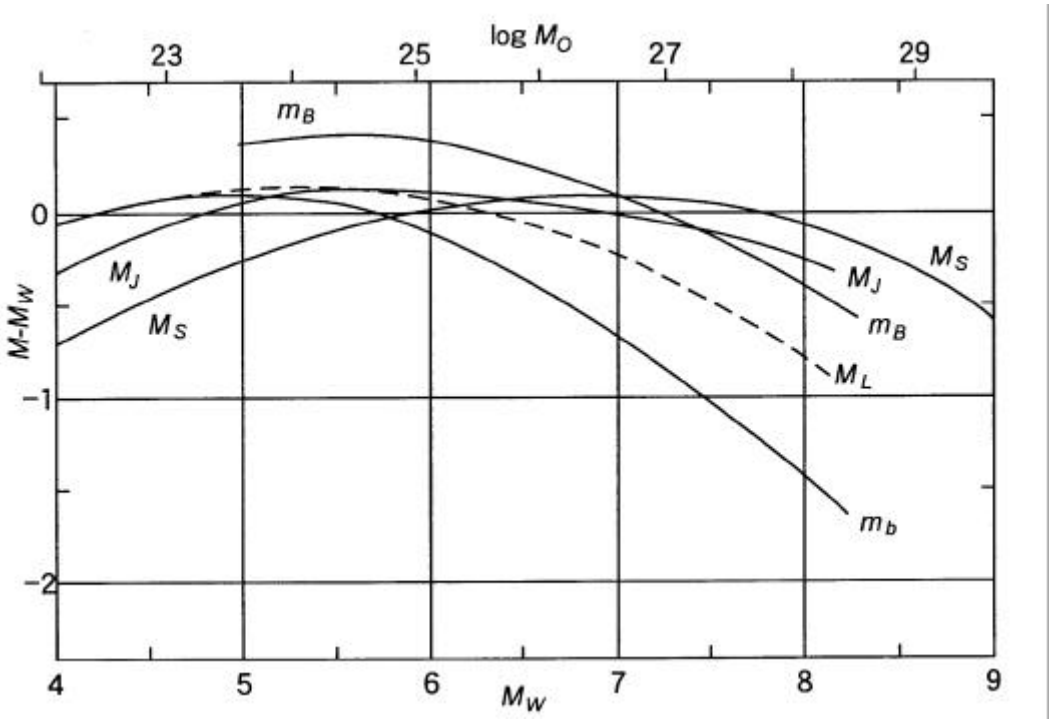

Figure 3.3.2 Relationship between Surface Wave Magnitude(Ms), Body Wave Magnitude(mb) and Moment Magnitude(Mw)

Source: Utsu (1982)

(4) Proposed Scenario Earthquake

Among the many active faults in the area, the most probable hazardous faults are the following:

- Mosha Fault (length: approximately 200km)
- North Tehran Fault (length: approximately 90km)
- South Ray Fault (length: approximately 20km).

The Mosha Fault is a major fault over 200km long, and it consists of several segments. The earthquake in 1830 corresponded to activity on the eastern segment of the Mosha Fault. Therefore, a part of the eastern Mosha Fault was selected as one of the scenario earthquake sources.

The largest historical earthquake occurred in 958 with Mw=7.7, at about 50km from the centre of Tehran. This earthquake corresponded to activity on the western segment of the Mosha Fault. The North Tehran Fault is located between the western segment of the Mosha Fault and the city of Tehran. If the North Tehran Fault is activated, the damage, which the resulting earthquake could cause, will be heavier than that which would be due to the re-occurrence of the event in 958. Thus, for the scenario earthquake, the North Tehran Fault should be considered instead of the western segment of the Mosha Fault.

The North Tehran Fault lies on the boundary between the northern mountainous area and the city area. This fault extends over 90 km, but the northwestern part of it is far from the city of Tehran. Therefore, the eastern part was selected as a source of one of the scenario earthquakes.

The South Ray Fault is located south of the city of Tehran, and its length is approximately 20 km. The whole length of this fault is modelled. The South Ray Fault extends along the south side of the Ray depression, and an almost parallel fault, named the North Ray Fault, extends along the north side of the depression. The interval between these two faults is only 3 to 5 km. It is considered that the root of these two faults is same and these are branches of one fault. It is difficult to say definitively because enough information on these faults is not available. Therefore, the model by the name of the ' Ray Fault Model' is used in this study. The South Ray Fault is modelled because of the better continuation of surface trace and higher micro seismic activity, but this model is representative of both the South Ray and North Ray Faults.

It should be noted that ' hidden' faults might exist underneath sediment layers of the city of Tehran. If such were the case, it would be difficult to determine their location, and the probability of occurrence would be the same anywhere in the city. To take into account this situation, the Floating Model concept can be considered.

In conclusion, the following four models for scenario earthquakes were considered:

- Ray Fault Model
- North Tehran Fault (NTF) Model
- Mosha Fault Model
- Floating Model

3.3.2. Earthquake Fault Model

(1) Dip Angle of the Fault

Several fault model parameters are necessary to calculate the seismic motion numerically. The length and azimuth of the faults are estimated from surface fault traces, and magnitude and length are estimated from an empirical formula. However, it is impossible to estimate the dip angle of the faults from available surface information because faults sometimes bend near the surface. Therefore, the dip angle of the fault is sometimes determined by the distribution of micro earthquake activities.

Figure 3.3.3 shows epicentral distribution of micro earthquakes around Tehran. Those data were provided from Institute of Geophysics, Tehran University (IGTU). The small squares indicate the epicentre observed from 1996 to 1999 by IGTU seismograph network. Figure 3.3.4 shows hypocentral distribution for depth along the cross section A-A' for Mosha Fault and B-B' for South Ray Fault. These hypocentres are correlated to the locations of earthquakes shown in black in Figure 3.3.3 and are assumed to have occurred along the faults. It was determined that the dip angle of this segment of the Mosha and the South Ray Faults was approximately 75 degrees to the north. On the other hand, dip angle of North Tehran Fault is assumed to be the same as that of the Mosha Fault, because there are no events along the fault.

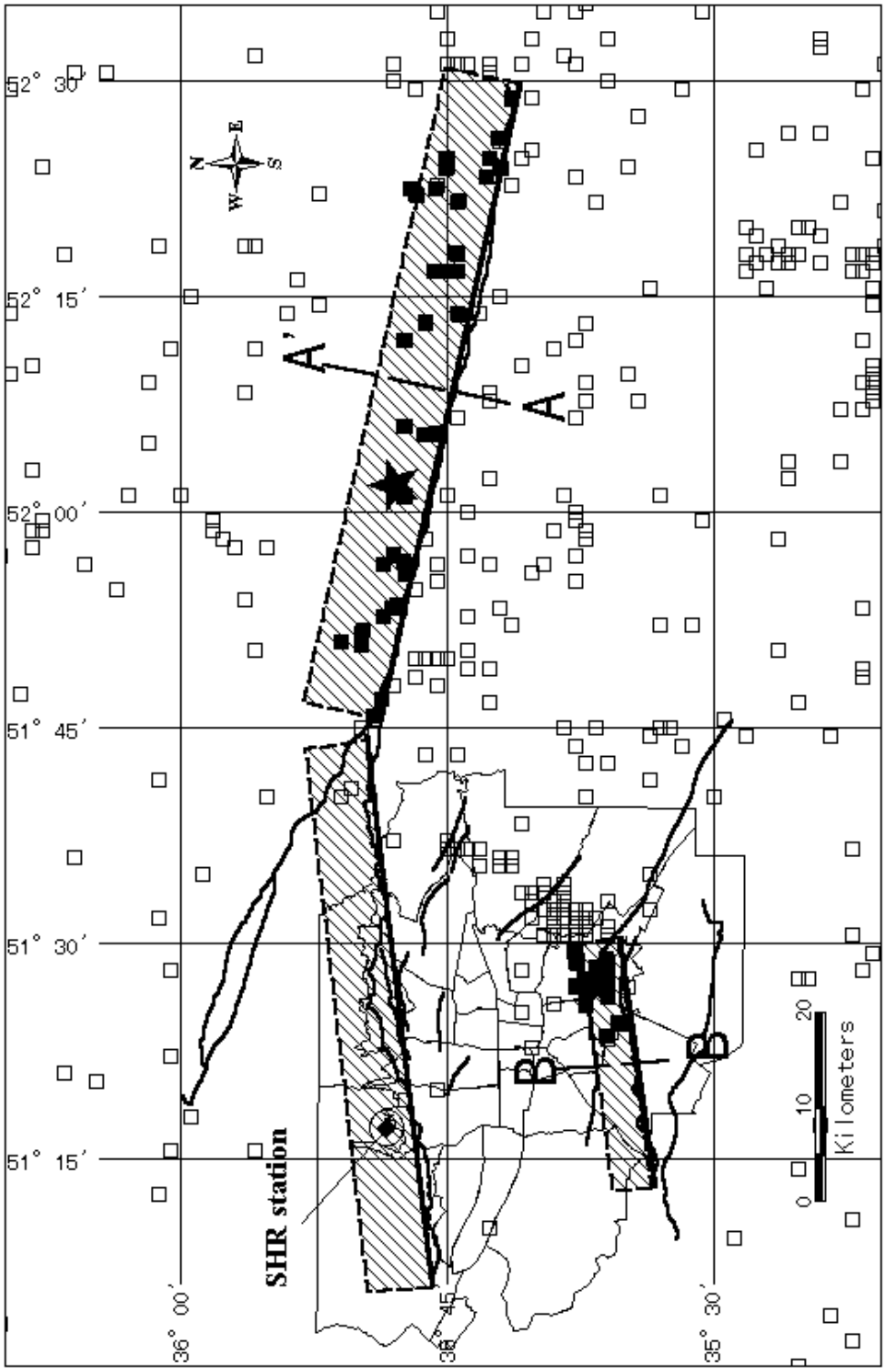

Figure 3.3.3 Distribution of Scenario Earthquakes

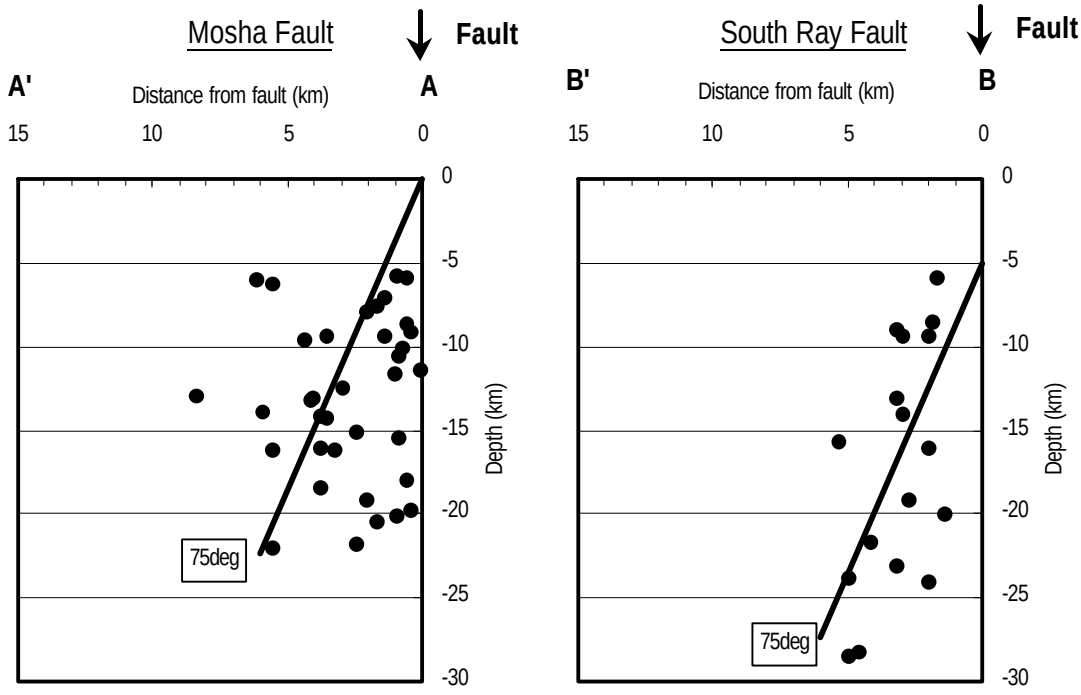

Figure 3.3.4 Estimated Dip Angle of Mosha Fault and South Ray Fault

Note: A', A, B' , B correspond to location of the cross section in Figure 3.3.3.

(2) Fault Model Parameters

Length, origin and azimuth of faults of the model were determined from surface fault traces of each fault. Length of the Floating model was set to half that of the Ray Fault model because the Floating model is the ' hidden' model. Width and magnitude were calculated from length using an empirical relation for reverse faults according to Wells and Coppersmith (1994).

Depth of the upper edge was assumed as 0 km for the Mosha Fault model and North Tehran Fault model. Depth of the upper edge was assumed as 5 km for the Ray Fault model and Floating Model because bedrock becomes deeper from north to south.

The projection of the fault model for scenario earthquakes is depicted by the hatched area in Figure 3.3.3. Details of the fault model parameter are summarised in Table 3.3.2.

Table 3.3.2 Fault Model Parameters

		Ray Fault model	NTF (North Tehran Fault) model	Mosha Fault model	Floating model
Length (km)		26	58	68	13
Width (km)		16	27	30	10
Moment Magnitude (Mw)		6.7	7.2	7.2	6.4
Origin	N (degrees)	35.8255	35.6815	35.5876	-
	E (degrees)	51.7392	52.4955	51.5061	-
Azimuth (Clockwise from North) (degrees)		263	263	283	263
Dip angle (degrees)		75	75	75	75
Depth of upper edge (km)		5	0	0	5

References for section 3.3

Berberian, M. M., Ghoreishi, B., Arajang R awesh, A. Mohajer Ashjai, 1983, Seismotectonic and earthquake fault hazard investigations in the Tehran region, Geological Survey of Iran, Report No. 56.

Berberian, M., and R. S. Yeats, 1999, Pattern of Historical Earthquake Rupture in the Iranian Plateau, Bull. Seism. Soc. Am., Vol.89, No.1.

Campbell, K.W., 1997, Empirical Near-Source Attenuation Relationships for Horizontal and Vertical Components of Peak Ground Acceleration, Peak Ground Velocity, and Pseydo-Absolute Acceleration Response Spectra, Seismological Research Letters, Vol.68, No.1.

Moinfar, A.A., Mahdavian, A. and Maleky, E., 1994, Historical and Instrumental Data Collection of Iran, Iranian cultural fairs institute.

Utsu, T., 1982, Relationships Between Earthquake Magnitude Scales, Bull. Earthq. Res. Inst., Vol.57. No.3, (in Japanese with English abstract).

Wells, D.L., and Coppersmith K.J., 1994, New Empirical Relationships among Magnitude, Rupture Length, Rupture Width, Rupture Area, and Surface Displacement, Bull. Seism. Soc. Am., Vol.84, No.4.

3.4. Analysis Methods

3.4.1. Synthesis of the Seismic Waveform at the Engineering Bed Rock

Observed earthquake motion can be modelled by the convolution of slip distribution in time and space domain at the fault surface and the response of materials in propagation pass for unit slip (Green's function). The idea of empirical Green's function is to use an observed small event as Green's function instead of a theoretical one to calculate a large event. The advantage of empirical Green's function is that a small event contains propagation-path effects and local site effects if the propagation-path of the small event is the same as that of a large event. Many researchers studied empirical Green's function method. In this study, Irikura (1986) was adopted.

To synthesise a large event from a small event, two similarity laws should be considered. One is the scaling relation of source parameters and the other is the scaling law of source spectra.

The source parameter relationships between large and small events are as follows:

$$\left(M_O / m_O\right)^{1/3} = L/l = W/w = N,$$

where, for large and small events, respectively, M_O and m_O are seismic moment, L and l are fault length, W and w are fault width. If large and small events obey ω^{-2} scaling, the spectral relationships between large and small events for the low-frequency and high-frequency ranges are as follows:

$$U_L / u_L = M_O / m_O = N^3, \quad U_H / u_H = \left(M_O / m_O\right)^{1/3} = N,$$

where U_L and u_L are the level of low-frequency range and U_H and u_H are the level of high-frequency range. With these relations, the seismogram $A(t)$ for large event is expressed in terms of the seismogram $a(t)$ of the small event as follows:

$$A(t) = \sum_{1}^{N^2} (r/r_i) F(t - t_i) * a(t),$$

$$F(t) = \delta(t) + (1/n') \sum_{j=1}^{(N-1)n'} \delta\left[t - (j-1)T/(N-1)n'\right],$$

$$t_i = r_i/Vc + \xi_i/Vr$$

where, r is the hypocentral distance from the observation point to the small event, r_i is the distance from the observation point to the ith fault element, ξ_i is the distance from the rupture nucleation point to the ith fault element, Vr is the rupture velocity, Vc is the velocity of seismic waves under consideration, T is the rise time of the large event, n' is the appropriate integer to eliminate spurious periodicity and * represents the convolution. A schematic illustration of this method is shown in Figure 3.4.1.

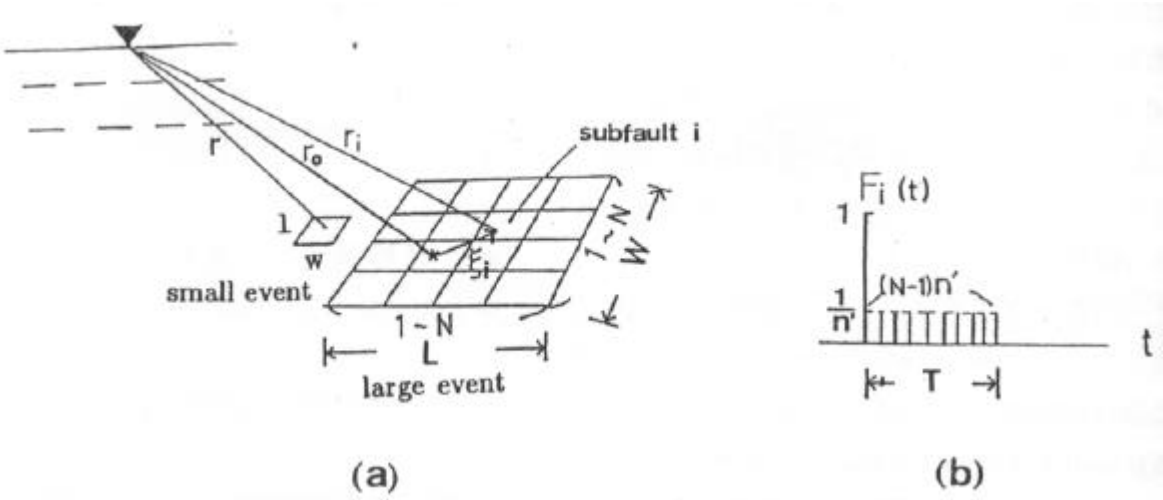

Figure 3.4.1 Schematic illustration of empirical Green's function method Irikura and Kamae (1992)

To synthesise the large event, i.e., the scenario earthquake, the following earthquake was used as the small event:

Date: March 18, 1997
Time: 05:35:54.70
Location: N35.80, E52.03
Magnitude: mb 3.9

The location of this earthquake is designated by a star in Figure 3.3.3. This earthquake is considered to have occurred on the Mosha Fault. The collected digital waveform data was supplied by IGTU. The frequency properties of the record are considered to be flat from 0.1 to 10 Hz. Therefore, the record was used without any kind of pre-treatment. The original velocity record was differentiated to an acceleration record numerically. The waveform is shown in Figure 3.4.2.

The waveform of the scenario earthquake was synthesised using the Irikura and Kamae (1992) method. Two steps of synthesis were applied because the difference of moment between the large event and the small event was too large for a one-step synthesis. Namely, the large earthquake of Mw 5.4 was first synthesised and then the scenario earthquake was synthesised from the Mw 5.4 earthquake.

The amplitude of the synthesised Mw 5.4 earthquake was too small compared to the expected value according to the empirical attenuation formula of Campbell (1997). Expected maximum acceleration was approximately 1.0 gal but amplitude of small earthquake (mb 3.9) is too small and maximum acceleration of the digital waveform was 0.07 gal. The reason for this discrepancy is not known at this time. In this analysis, the amplitude of the Mw 5.4 synthesised earthquake was fitted to the empirically expected value according to Campbell (1997).

The synthesis was done for each 500 m square mesh. With regards to the Floating model, only one waveform was calculated for a large earthquake. An example of the synthesised waveform is shown in Figure 3.4.3. The subsurface amplification that is mentioned in the next chapter is included in the waveform.

The parameters that were used in the analysis of waveform synthesis are shown in Table 3.4.1.

Table 3.4.1 The Parameters for Green' s Function Method

Parameters		1st. step	2nd. Step			
			Ray Fault model	NTF model	Mosha Fault model	Floating model
Main Fault	Strike (degrees)	257	277	277	257	277
	Dip (degrees)	45	75	75	75	75
	Rake Angle (degrees)	90	90	90	90	90
	Depth (km)	3.9	19.1	24.4	26.9	13.5
Small Fault	Strike (degrees)	257	257	257	257	257
	Dip (degrees)	45	45	45	45	45
	Rake Angle (degrees)	90	90	90	90	90
	Depth (km)	18.5	3.9	3.9	3.9	3.9
N		5	5	8	9	3
Initial rupture point		east of lower end	centre of lower end	centre of lower end	east of lower end	centre of lower end
Shear Wave Velocity (km/s)		3.0	3.0	3.0	3.0	3.0
Rupture Propagation Velocity (km/s)		2.16	2.16	2.16	2.16	2.16

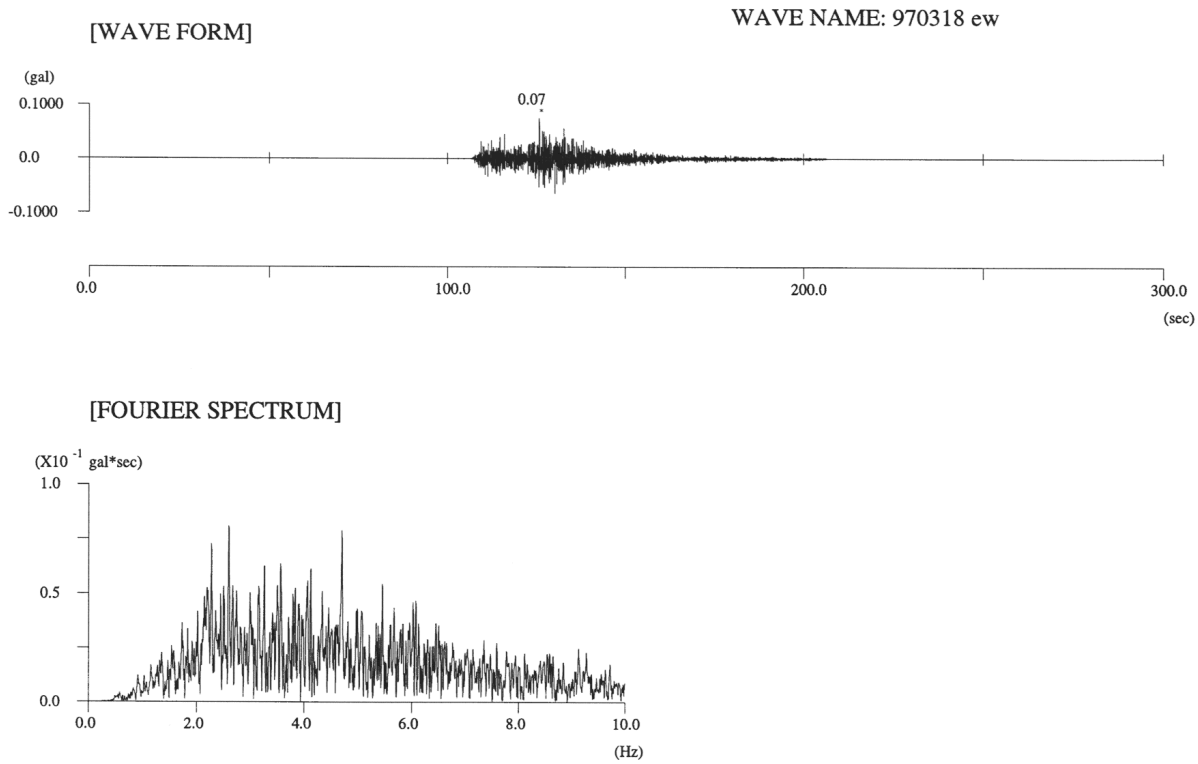

Figure 3.4.2 Waveform of Small Event

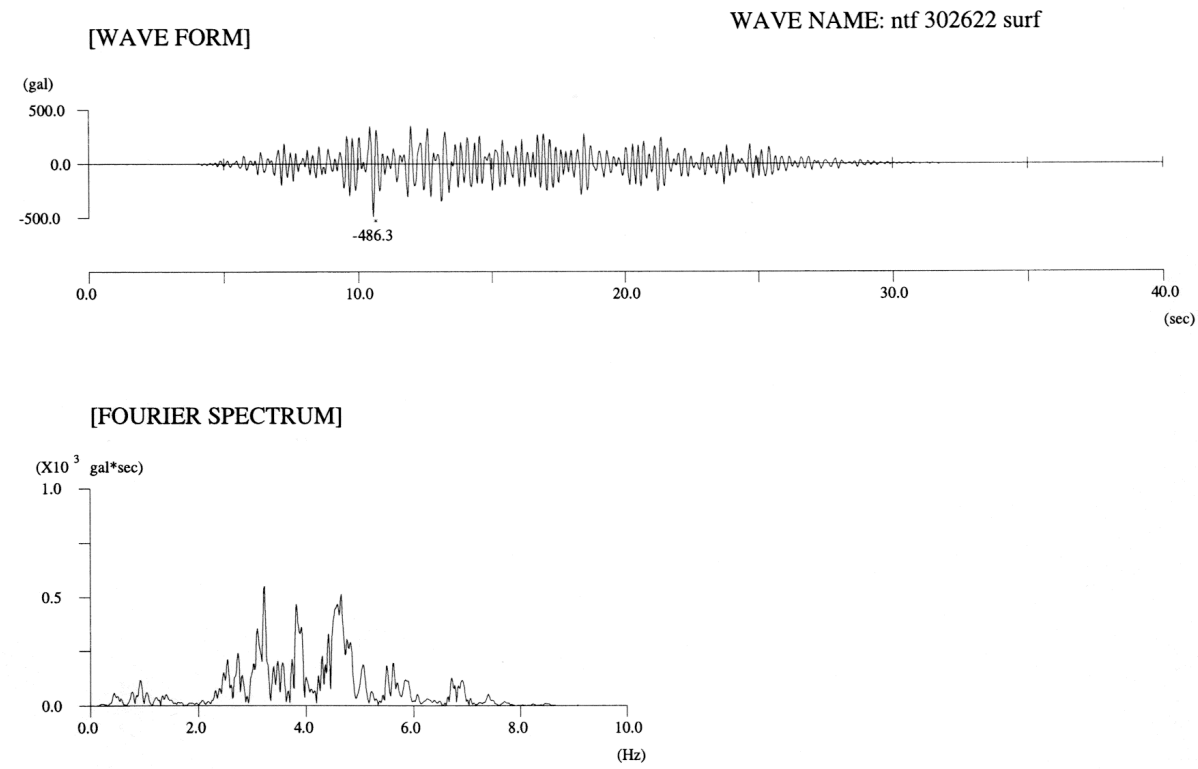

Figure 3.4.3 Synthesised Waveform

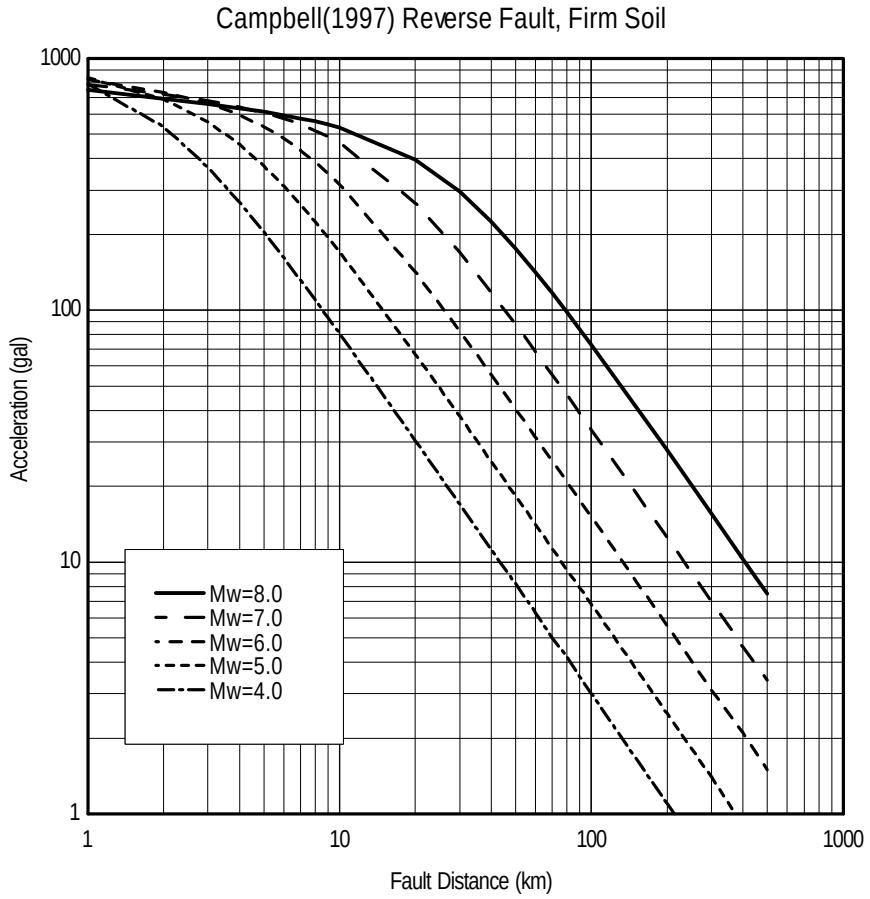

Figure 3.4.4 Relationship between Acceleration and Fault Distance

Source: Campbell (1997)

3.4.2. Amplification of Subsurface Ground

The amplification of the subsurface was analysed using a one-dimensional response analysis. The non-linearity effect was not considered because the soil is stiff enough to neglect the non-linearity. The S-wave velocity of most of the soft soil in Tehran is over 340m/sec; this type of layer is treated as the foundation of building in many cases. For example, in the blind prediction test of ESG1992 (International Symposium on the Effect of Surface Geology on Seismic Motion), the dynamic deformation characteristics of the layer of Vs over 400m/sec was considered to be linear.

Based on the ground classification and soil properties, a ground model for the response analysis was made. An example of the model is shown in Table 3.4.2. Dumping factors were set to 2% after Ohta (1983), taking into account the Vs value as shown in Figure 3.4.5. The amplification function for each ground model calculated with the response analysis is shown in Figure 3.4.6, Figure 3.4.7.

Table 3.4.2 Example of Ground Model for Response Analysis (Ground Model No. 7)

Depth (m)	Vs (m/sec)	Density (g/cm^3)	Dumping (%)
0-10	340	2.0	2
10-50	430	2.0	2
50-70	530	2.0	2
70-	580	2.0	---

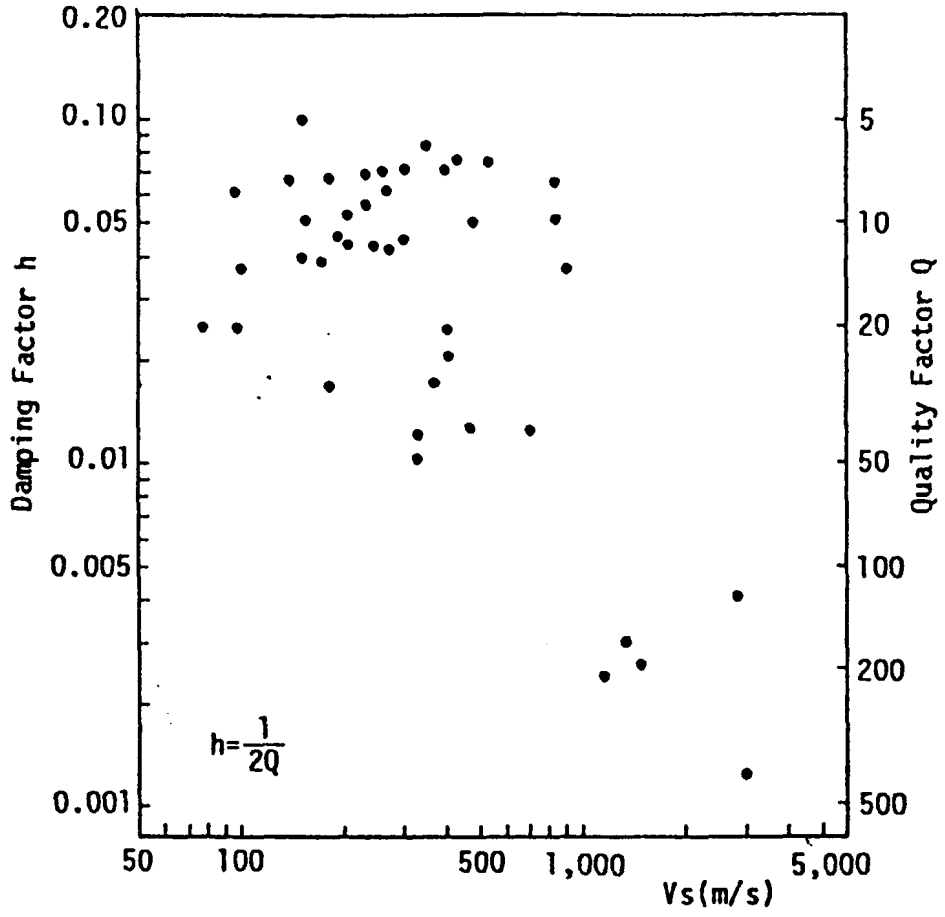

Figure 3.4.5 Relationship between Dumping Ratio and Shear Wave Velocity

Source: Ohta (1983)

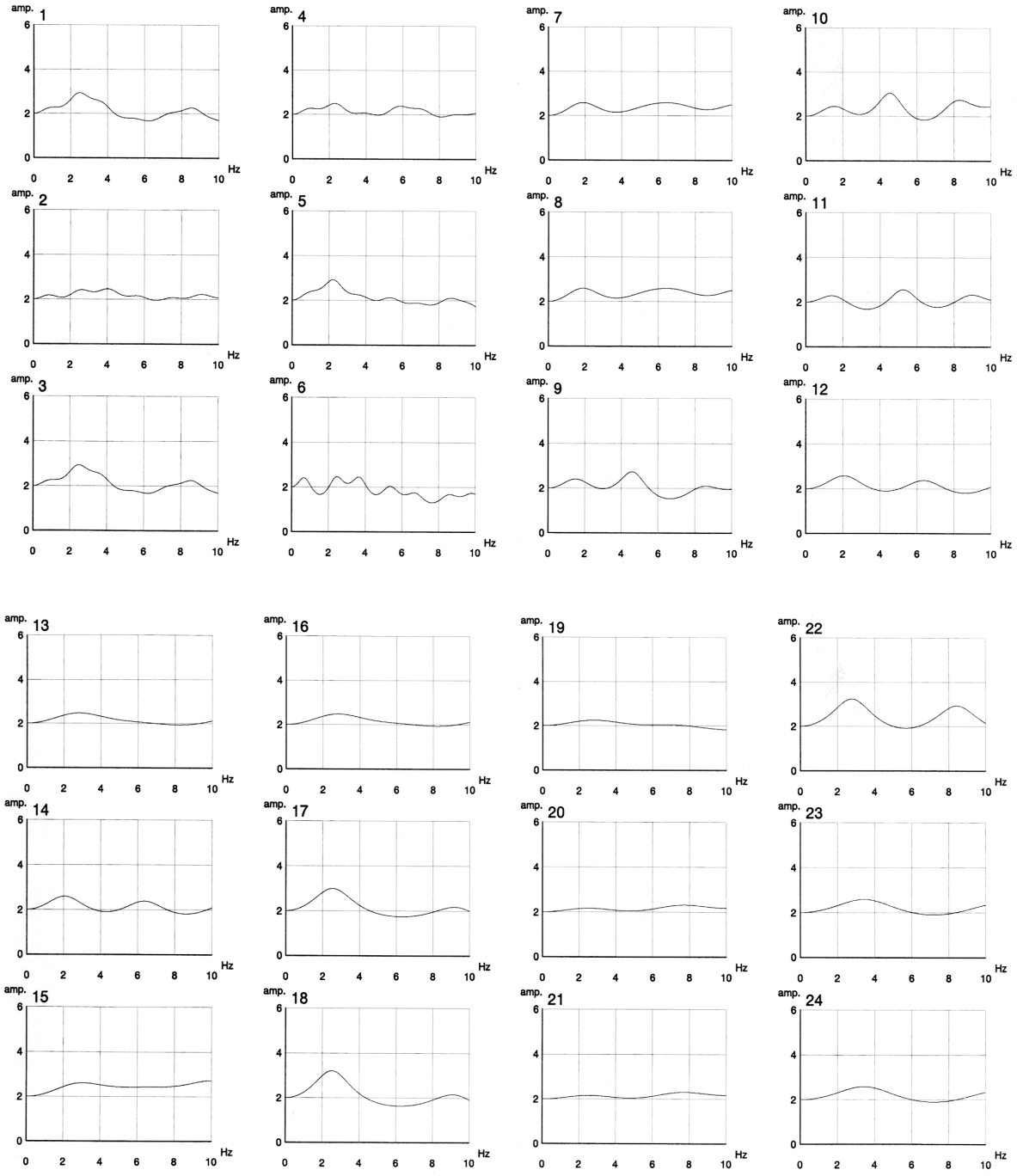

Figure 3.4.6 Amplification Function in Frequency Domain (1)

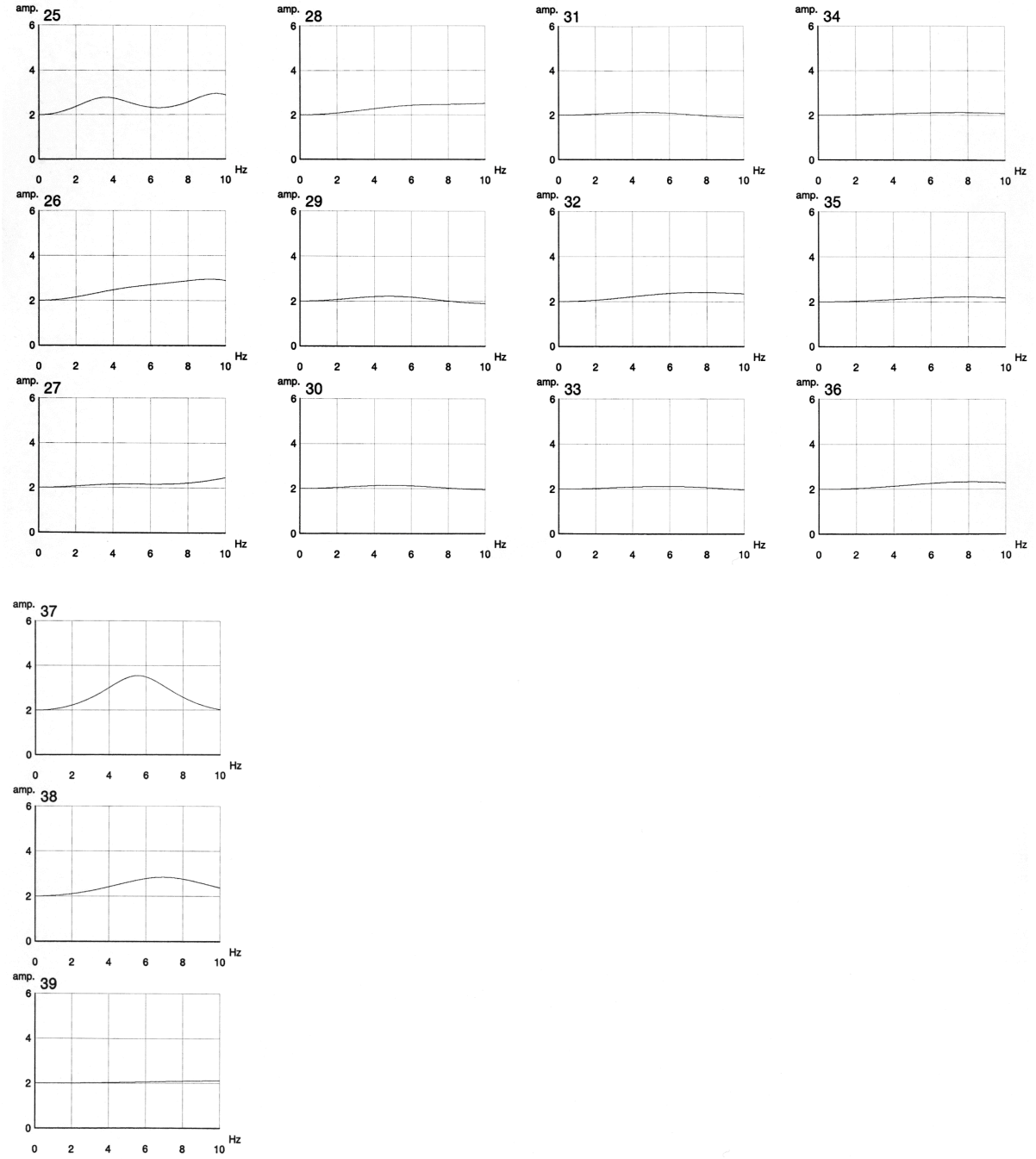

Figure 3.4.7 Amplification Function in Frequency Domain (2)

References for section 3.4

Campbell, K.W., 1997, Empirical Near-Source Attenuation Relationships for Horizontal and Vertical Components of Peak Ground Acceleration, Peak Ground Velocity, and Pseydo-Absolute Acceleration Response Spectra, Seismological Research Letters, Vol.68, No.1.

Irikura, K., 1986, Prediction of Strong Ground Motions using Empirical Green' s Function, Proc. 7th Japan Earthq. Eng. Symp.

Irikura, K. and K. Kamae, 1992, Some Problems in Practical Applications of Strong Motion Prediction, Programme and Abstracts, The Seismological Society of Japan 1992 Fall Meeting, (in Japanese).

Ohta, T, 1983, Section 4.3 Kinetics of Ground, Earthquake Motion and Ground Condition, AIJ,(in Japanese).